

Electronic Supporting Information (ESI) for:

Titanium nanoparticles (TiO₂) / Graphene oxide nanosheets (GO): an electrochemical sensing platform for the sensitive and simultaneous determination of benzocaine in the presence of antipyrine

Mona A. Mohamed*¹, Shima A. Atty¹, Hanan A. Merey², Taghreed A. Fattah¹,
Christopher W. Foster³ and Craig E. Banks*³

¹Pharmaceutical Chemistry Department, National Organization for Drug Control and Research (NODCAR), Giza, Egypt

²Analytical Chemistry Department, Faculty of Pharmacy, Cairo University, Cairo, Egypt

³Faculty of Science and Engineering, Manchester Metropolitan University, Chester Street, Manchester M1 5GD, UK

*To whom correspondence should be addressed.

E-mail: nodcar1977@yahoo.com and c.banks@mmu.ac.uk;

Characterisation of TiO₂-GO used in the fabrication of the electrochemical sensors

The TiO₂-GO was fabricated as detailed in the experimental section. Figure S1A depicts typical SEM images of the TiO₂ nanoparticles, SEM of GO nanosheets and TiO₂-GO nanocomposite. The TiO₂ nanoparticles appear spherical in nature with average diameter of 100 nm (Figure S1A). Figure S1B shows the formation of GO structures which are agglomerated into micron sized flasks/clusters. Graphene oxide provides a large surface area and surface to electrically wire the TiO₂.¹⁻⁴ Figure S1C shows the TiO₂-GO which appear to be well distributed and incorporated over the GO nanosheets. The crystal structure of the synthesized materials was investigated by XRD; Figure 1D. The XRD pattern of GO exhibits a typical (002) GO peak at $2\theta = 10^\circ$. The graphite flakes, used as a precursor for the fabrication of GO, exhibit a strong and sharp peak at 26.26° , indicating a highly ordered structure⁵ which agrees with independent literature confirming the presence of GO.

The FTIR spectra of GO, TiO₂, and TiO₂-GO are reported in Figure S2. The FT-IR spectrum of the GO confirms the successful oxidation of graphite. Additionally the broad and wide peaks at 3439 and 1719 cm^{-1} are attributed to the oxygen-containing functional groups on the graphite oxide⁶, confirming the presence of different types of oxygen functionalities in GO⁷. While the absorption band at 1560 cm^{-1} can be ascribed to benzene rings⁸, the sharp intense peak at 1419 cm^{-1} can be attributed to CO-carboxylic. The spectrum of the prepared TiO₂ (Figure S2), 600 and 1200 cm^{-1} are assigned to Ti-O-Ti and Ti-O stretching, respectively. 3290 cm^{-1} is due to O-H stretching, which means that the TiO₂ nanocrystal is easily absorbs water in the air⁹. In the spectrum of TiO₂-GO (Figure S2), the broad band between 900 – 1860 cm^{-1} is characteristic of TiO₂-O stretching in a TiO₂-based composite. Furthermore, we find that most of the peaks in the spectra of GO and TiO₂ still exist. These findings support that the preparation of TiO₂ successfully incorporated GO.

The x-ray photoelectron spectroscopy (XPS) data was acquired using a bespoke ultra-high vacuum system fitted with a *Specs GmbH Focus 500 monochromated Al K α* X-ray source, *Specs GmbH Phoibos* 150 mm mean radius hemispherical analyser with 9-channeltron detection, and a *Specs GmbH FG20* charge neutralising electron gun. The GO was observed to contain 68.8 % carbon and 26.6 % oxygen with trace amounts of nitrogen, sulphur and chlorine which are likely contaminants from the fabrication process. Further analysis found the GO to correspond to graphitic C-C bonding in addition to C-O or C-O-C bonds (47.21 %, 286.7 eV) and C=O or COO

(7.94 %, 288.4 eV) bonds where characteristically present, which is in excellent agreement with previous literature reports.

Figure S1: SEM imaging of TiO₂ (A), GO (B), and TiO₂-GO (C). Additionally presented is XRD spectra of GO compared to a graphite control sample (D).

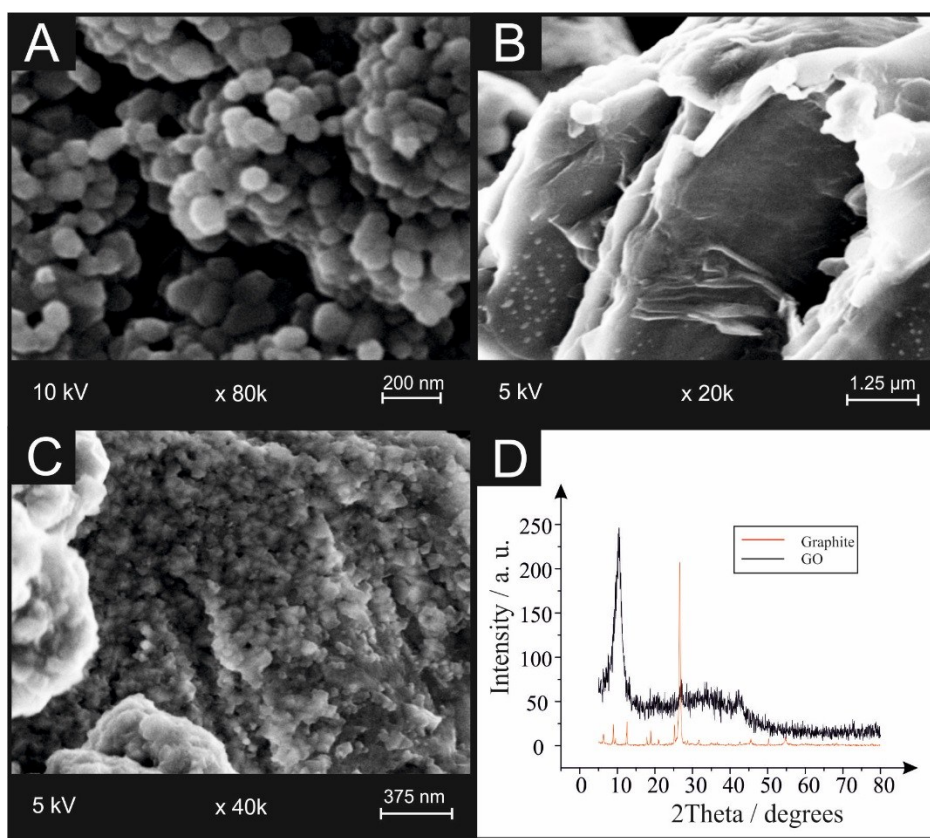
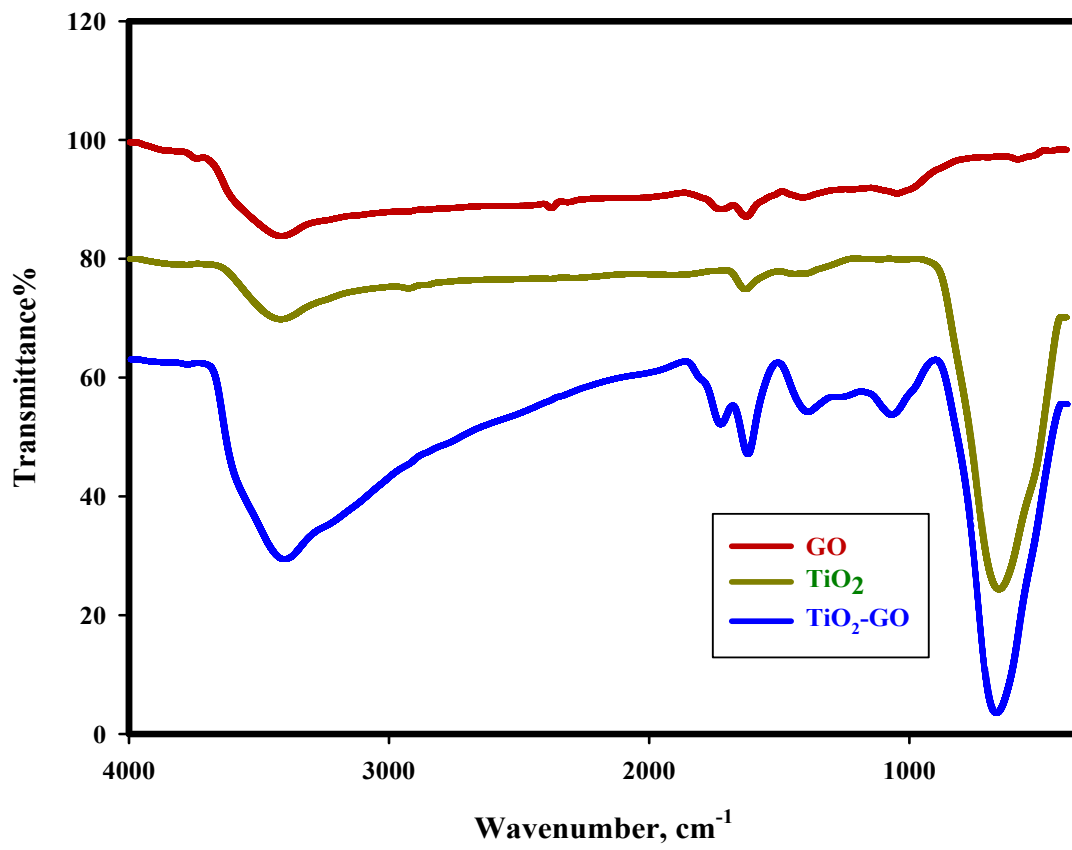


Figure S2. FTIR spectra of GO, TiO₂, and TiO₂-GO.



The electroactive areas of the electrodes used in this paper were deduced via cyclic voltammetry from monitoring the peak current as a function of applied voltammetric scan rate in the following solution: 5.0 mM $\text{K}_3\text{Fe}(\text{CN})_6$ / 0.1 M KCl; Figure S3 shows typical voltammetric responses. The electrode areas were determined from the Randles-Ševčík equation for an irreversible process ¹⁰:

$I_p = 2.65 \times 10^5 n^{\frac{3}{2}} A D^{\frac{1}{2}} C v^{\frac{1}{2}}$ where I_p is the peak current, n is the number of electrons transferred in the electrochemical process, A is the electrode area, D is the diffusion coefficient, C is the redox probe concentration and v is the applied voltammetric scan rate. The used D value used was¹¹: $7.6 \times 10^{-6} \text{ cm}^2 \text{ s}^{-1}$. The electroactive area was calculated from the slope of the plot of I_p versus $v^{1/2}$ and the calculated areas were found to correspond to 0.055, 0.074, 0.095 and 0.144 cm^2 for CPE, TiO_2/CPE , and GO/CPE , and $\text{TiO}_2\text{-GO}/\text{CPE}$, respectively.

Figure S3. Cyclic voltammograms recorded using CPE, GO/CPE, TiO₂/CPE, and TiO₂-GO/CPE sensors. Solution composition: 5.0 mM K₃Fe(CN)₆ / 0.1 M KCl. Scan rate: 100 mV s⁻¹

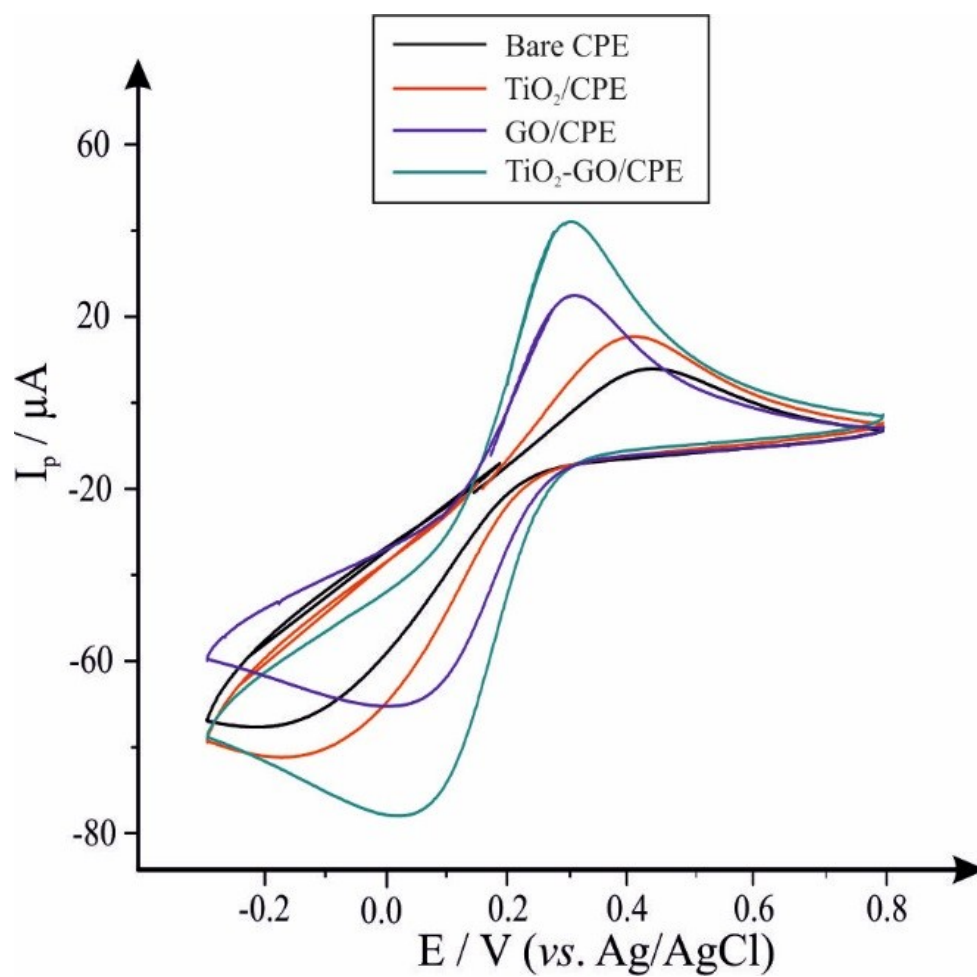
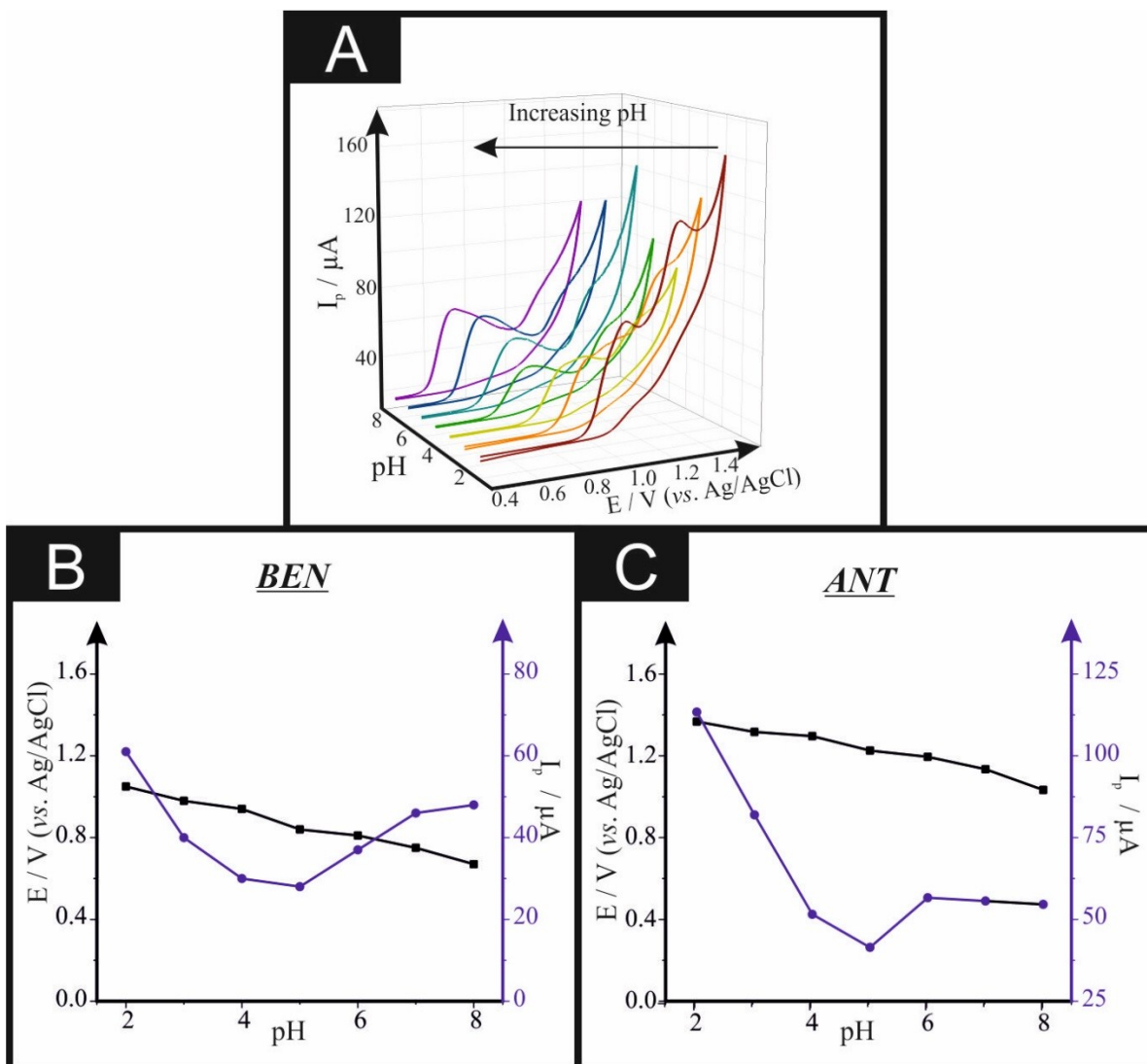


Figure S4. Cyclic voltammetric responses of 1.0 mM BEN and ANT over a range of pH values using TiO₂-GO/CPE sensing platforms. Scan rate: 0.1 V s⁻¹. (B) and (C) depict analysis of the oxidation peak current (circles) and peak potential (squares) of BEN and ANT as a function of pH variations.



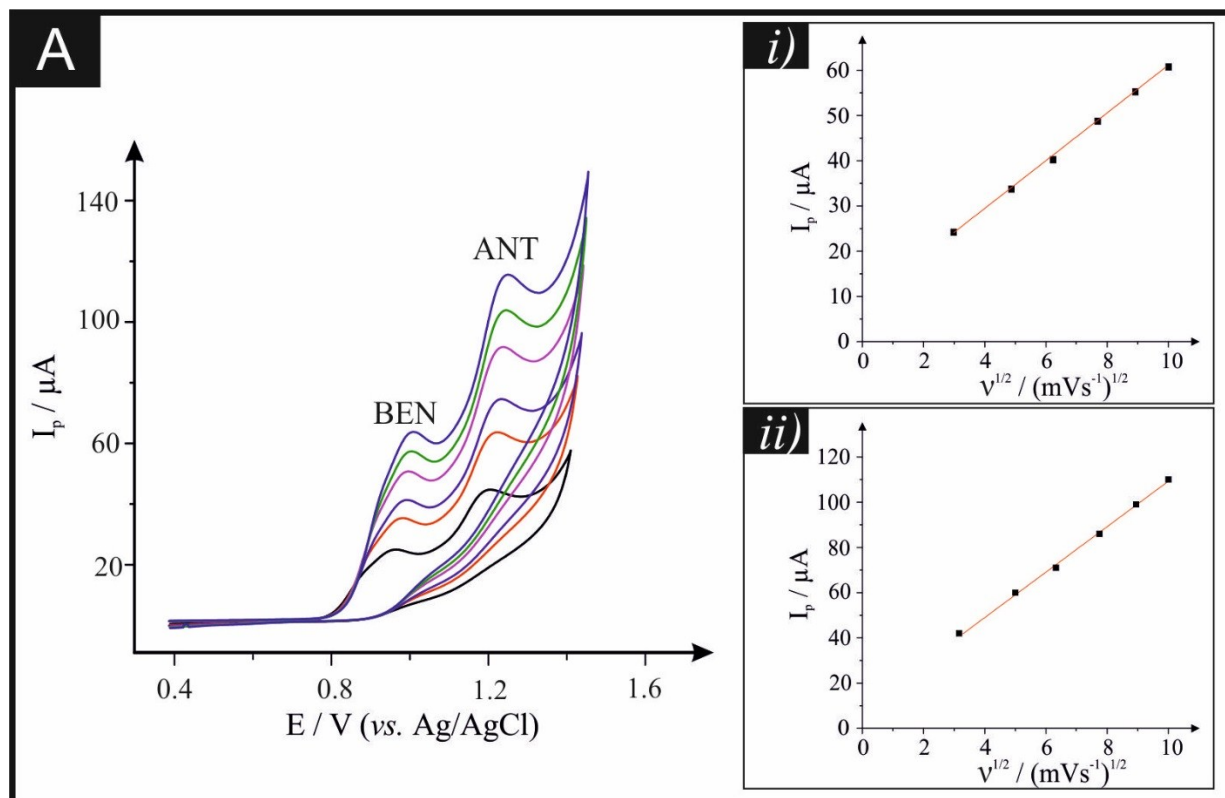
The effect of changing the voltammetric scan rate upon the electrochemical oxidation of BEN and ANT was studied using cyclic voltammetry. The influence of scan rate (ν) on the electrochemical response ($I_{p,a}$) using TiO₂-GO/CPE sensing platforms was recorded in 1.0 mM BEN and ANT with the results shown in Figure S5. The results indicate that the anodic peak currents change linearly with the square root of scan rate ($\nu^{1/2}$) for BEN and ANT:

$$I_{p,a} (\mu\text{A}) = 5.30 \nu^{1/2} + 6.16 (R^2 = 0.9996) \text{ (For BEN)}$$

$$I_{p,a} (\mu\text{A}) = 9.92 \nu^{1/2} + 9.80 (R^2 = 0.9992) \text{ (For ANT)}$$

This suggests that the electrochemical process is diffusion-controlled for the electrochemical oxidation of BEN and ANT using the TiO₂-GO/CPE over the studied range of potential scan rates (10 – 100 mV s⁻¹).

Figure S5. Cyclic voltammograms of 1.0 mM of BEN and ANT in BRB (pH 2.0) using a TiO₂-GO/CPE sensor recorded at various scan rates: 10 - 100 mVs⁻¹. Inset *i* & *ii*: plot of I_p vs. $v^{1/2}$ for BEN and ANT, respectively.



The chronoamperometric measurements, as shown in Figures S6 and S7, of BEN and ANT were performed at a constant applied DC potential at TiO₂-GO/CPE in pH 2.0 BRB with the current–time profiles obtained by setting the working electrode potential at +1.02 and +1.21 V (vs. Ag/AgCl) respectively for various concentrations of BEN and ANT. The inset shows the plots of currents, sampled at fixed time as a function of BEN concentrations, added to the blank solution at different times after the application of the potential step. For an electroactive material with the diffusion coefficient (D), the current corresponding to the electrochemical reaction (under diffusion control) is described by Cottrell's law ¹²:

$$I(t) = nFAC \cdot \left(\sqrt{\frac{D}{\pi t}} \right)$$

The level of the Cottrell current, measured for 30 s, increased by increasing BEN concentration. The plot of I versus $t^{-1/2}$, showed a straight line (inset) and from its slope, the value of D can be obtained. According to the Cottrell equation, the slope of fixed time current versus BEN and ANT concentration plots is $nFA(D/\pi t)^{1/2}$, which can provide diffusion coefficients of BEN and ANT, which were calculated to be $4.95 \times 10^{-6} \text{ cm}^2 \text{ s}^{-1}$ and $2.34 \times 10^{-6} \text{ cm}^2 \text{ s}^{-1}$, respectively.

Figure S6. Chronoamperograms for the oxidation of increasing concentrations of BEN at TiO₂-GO/CPE in pH 2 BRB. Potential step: +1.01 (vs. Ag/AgCl) respectively. Inset *i* shows the variation of chronoamperometric currents at $t = 30$ s vs. [BEN] concentration. The values 1 to 5 in Cottrell's plot (inset *ii*) correspond to 21.74 to 134.60 μM of BEN.

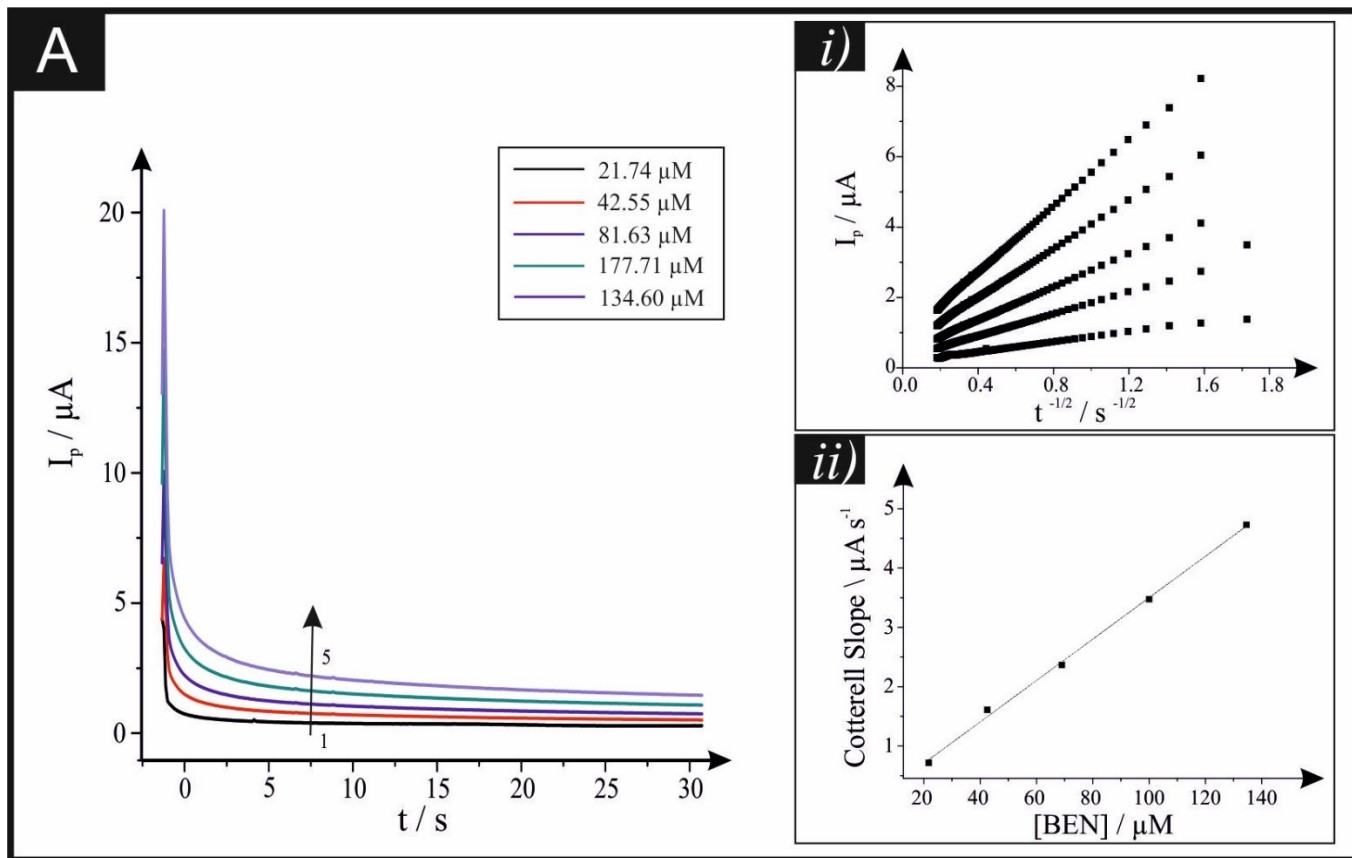


Figure S7. Chronoamperograms for the oxidation of increasing concentrations of ANT at the TiO₂-GO/CPE in pH 2 BRB. Potential step: +1.28 V (vs. Ag/AgCl) respectively. Inset *i* shows the variation of chronoamperometric currents at $t = 30$ s vs. [ANT] concentration. The values 1 to 5 in Cottrell's plot (inset *ii*) correspond to 21.74 to 134.60 μM of ANT.

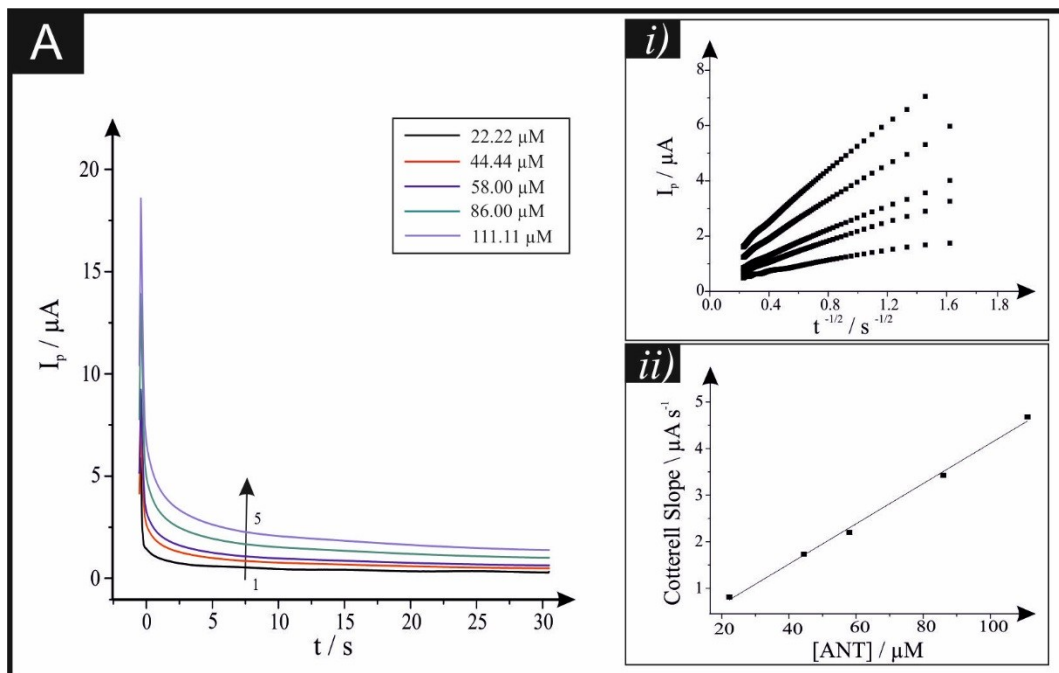


Figure S8. (A) Cyclic voltammograms for six measurements of 0.1 mM BEN and ANT; (B) Cyclic voltammograms using three different TiO₂-GO/CPE of 0.1 mM BEN and ANT.

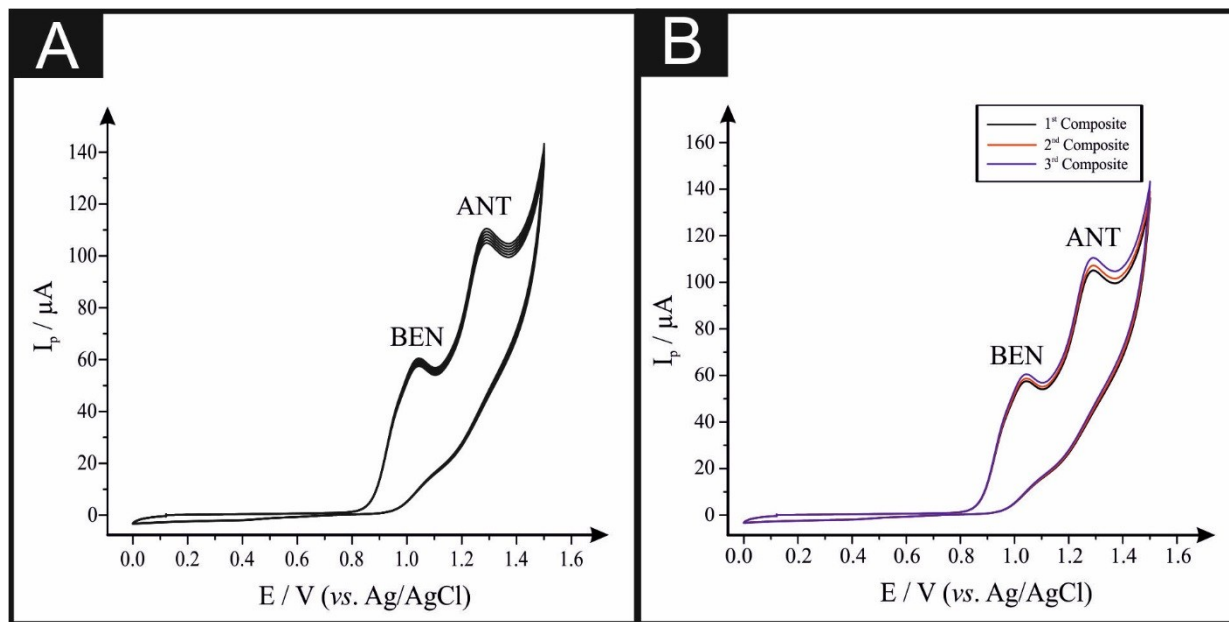


Table S1. Inter- and Intra- day precision of the developed sensing protocol.

Drug	Concentration, M	Inter-day RSD% ^a	Intra-day RSD% ^b
ANT	50.0×10^{-6}	2.45	2.67
	20.0×10^{-5}	1.98	2.01
	1.0×10^{-3}	1.52	1.99
BEN	50.0×10^{-6}	2.53	2.78
	20.0×10^{-5}	1.88	1.97
	1.0×10^{-3}	1.68	1.77

^a Average of 5 determinations

^b Average of 15 determinations over 3 days

References

1. Q. Quan, X. Lin, N. Zhang and Y.-J. Xu, *Nanoscale*, 2017, 9, 2398-2416.
2. M.-Q. Yang, N. Zhang, Y. Wang and Y.-J. Xu, *Journal of Catalysis*, 2017, 346, 21-29.
3. Y. Zhang, Z.-R. Tang, X. Fu and Y.-J. Xu, *ACS nano*, 2010, 4, 7303-7314.
4. N. Zhang, M.-Q. Yang, S. Liu, Y. Sun and Y.-J. Xu, *Chem. Rev.*, 2015, 115, 10307-10377.
5. S. Bykkam, K. Rao, C. Chakra and T. Thunugunta, *Int. J. Adv. Biotechnol. Res*, 2013, 4, 142.
6. L. Tang, Y. Wang, Y. Li, H. Feng, J. Lu and J. Li, *Advanced Functional Materials*, 2009, 19, 2782-2789.
7. T. Zhang, D. Zhang and M. Shen, *Materials Letters*, 2009, 63, 2051-2054.
8. Y. Si and E. T. Samulski, *Nano letters*, 2008, 8, 1679-1682.
9. J. Shen, B. Yan, M. Shi, H. Ma, N. Li and M. Ye, *Journal of Materials Chemistry*, 2011, 21, 3415-3421.
10. R. G. Compton and C. E. Banks, *Understanding voltammetry*, World Scientific, 2007.
11. W. Vielstich, *Berichte der Bunsengesellschaft für physikalische Chemie*, 1972, 76, 368-369.
12. A. J. Bard, L. R. Faulkner, J. Leddy and C. G. Zoski, *Electrochemical methods: fundamentals and applications*, Wiley New York, 1980.